SPECIAL
DYNAMO/CINDY/AMIE/LASP
COLLECTION

Variations of the Moist Static Energy Budget of the Tropical Indian Ocean Atmospheric Boundary Layer

SIMON P. DE SZOEKE

College of Earth, Ocean, and Atmospheric Sciences, Oregon State University, Corvallis, Oregon

(Manuscript received 21 November 2017, in final form 20 February 2018)

ABSTRACT

The atmospheric circulation depends on poorly understood interactions between the tropical atmospheric boundary layer (BL) and convection. The surface moist static energy (MSE) source (130 W m^{-2}, of which 120 W m^{-2} is evaporation) to the tropical marine BL is balanced by upward MSE flux at the BL top that is the source for deep convection. Important for modeling tropical convection and circulation is whether MSE enters the free troposphere by dry turbulent processes originating within the boundary layer or by motions generated by moist deep convection in the free troposphere. Here, highly resolved observations of the BL quantify the MSE fluxes in approximate agreement with recent cloud-resolving models, but the fluxes depend on convective conditions. In convectively suppressed (weak precipitation) conditions, entrainment and downdraft fluxes export equal shares (60 W m^{-2}) of MSE from the BL. Downdraft fluxes are found to increase 50%, and entrainment to decrease, under strongly convective conditions. Variable entrainment and downdraft MSE fluxes between the BL and convective clouds must both be considered for modeling the climate.

1. Introduction

Processes that control the moist static energy (MSE) of the boundary layer (BL) determine updraft buoyancy, affecting deep convection that drives the atmospheric circulation (Raymond 1995; Neelin and Zeng 2000; DeMott et al. 2015). Climate models with stronger mixing of water vapor between the atmospheric BL and the free troposphere have stronger positive low-cloud feedback and stronger climate sensitivity to greenhouse gases (Sherwood et al. 2014), yet the mechanism for this mixing is unknown. Model cumulus parameterizations initialize buoyant updrafts with air properties from the BL (e.g., Arakawa and Schubert 1974; Betts 1976; Zhang and MacFarlane 1995; Mapes 2000; Fletcher and Bretherton 2010). Recent cloud-permitting models simulated an entrainment sink of BL MSE that slightly exceeded that due to downdrafts (Thayer-Calder and Randall 2015).

Turbulent flux from the ocean surface, mostly evaporation, supplies the BL with MSE. The BL transports MSE to the free troposphere in cumulus updrafts and entrains warm dry free-tropospheric air and cold nearly saturated downdrafts from convection (Fig. 1).

In the Dynamics of the Madden–Julian Oscillation (DYNAMO; Yoneyama et al. 2013) field experiment in the central Indian Ocean (0°, 80°E), the BL was topped by a nearly moist adiabatic cumulus layer with cloud bases at 500–1000 m. This study diagnoses the BL MSE budget for the relatively mixed BL below the BL depth, z_i = 500 m (Fig. 1), during suppressed, disturbed, and active phases of the intraseasonal Madden–Julian oscillation (MJO; Madden and Julian 1971). Mass and MSE fluxes due to entrainment and downdrafts are estimated from in situ measurements of conserved variables—potential temperature θ and specific humidity q—as described in section 2. The MSE fluxes and their variation with the MJO are presented in section 3, and section 4 summarizes our findings.

2. A method for diagnosing the sources of BL air

The downdraft and entrainment MSE fluxes are calculated from the observed surface MSE flux and the

Denotes content that is immediately available upon publication as open access.

Corresponding author: Simon P. de Szoeke, sdeszoek@coas.oregonstate.edu

DOI: 10.1175/JAS-D-17-0345.1

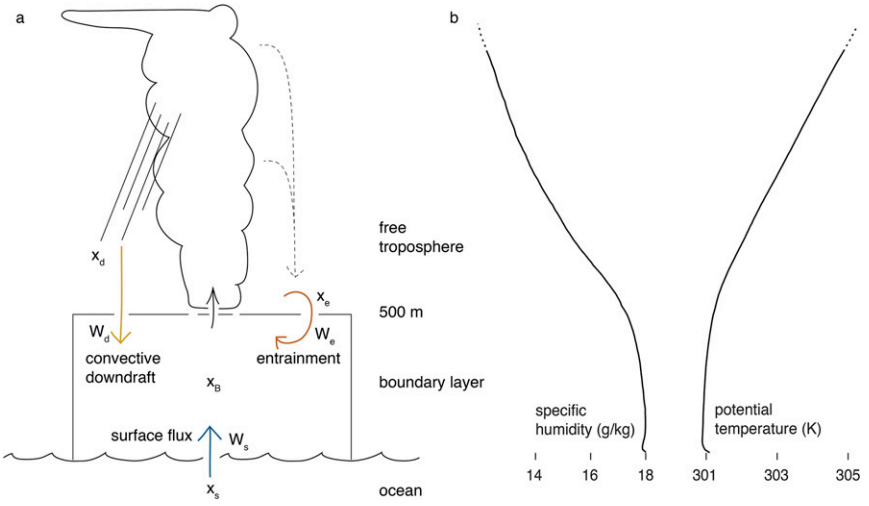

FIG. 1. (a) Schematic of fluxes from the surface, downdrafts, and entrainment responsible for the budget of a conserved variable x in the mixed BL. (b) Mean specific humidity and potential temperature soundings to scale for the schematic BL for when the surface air was not influenced by downdrafts (surface temperature >27.5°C).

mixing fractions of three end members, or sources of air that contribute their properties to the boundary layer. At equilibrium, a conserved variable in the BL (e.g., MSE h_B) is the sum of the downdraft (d), entrainment (en), and surface (s) end members weighted by their respective mass mixing fractions:

$$h_B = f_d h_d + f_{\rm en} h_{\rm en} + f_s h_s . \qquad (1)$$

Next, we describe the observations and the transformation from conserved variables to mixing fractions and MSE (de Szoeke et al. 2017).

a. *In situ observations*

Estimates of the BL θ_B and q_B and θ_d, $\theta_{\rm en}$, θ_s, q_d, $q_{\rm en}$, and q_s of end members (and thus h_B, h_d, $h_{\rm en}$, and h_s) are made each minute from two monthlong time series of in situ observations of temperature and humidity at 15 m from legs 2 and 3 of the Research Vessel *Roger Revelle* during the DYNAMO experiment in October–December 2011 (de Szoeke et al. 2015, 2017). Potential temperature θ_B and specific humidity q_B are extrapolated from the measurement height (15 m) in the surface layer to 100 m by flux–gradient similarity theory. The ocean surface end-member properties θ_s and q_s are calculated from the ocean skin temperature and its saturation specific humidity. Surface sensible and latent heat and MSE fluxes are computed using the COARE 3.5 bulk aerodynamic algorithm (Edson et al. 2013).

Turbulence entrains unsaturated air from the base of the cumulus layer into the BL. We choose properties $\theta_{\rm en}$ and $q_{\rm en}$ of the entrainment end member from 800-m altitude, where the mean θ sounding is moist adiabatic ($>4\,{\rm K\,km^{-1}}$) compared to the well-mixed BL (lapse rate $< 2\,{\rm K\,km^{-1}}$). We interpolate the 3-hourly soundings (Johnson and Ciesielski 2013; Ciesielski 2014) to the high resolution of the surface measurements. The potential temperature is relatively constant among soundings, but the specific humidity varies.

Downdrafts cooled to saturation by evaporation of rain or detrained cloud water conserve wet-bulb potential temperature (e.g., Zuidema et al. 2012). Soundings of free-tropospheric wet-bulb potential temperature are relatively uniform with height. Most of the BL potential temperature variability is due to cold pools with wet-bulb potential temperature representative of the lower to midtroposphere (de Szoeke et al. 2017). We estimate θ_d of downdrafts as the 2.5–3.5-km mean wet-bulb potential temperature θ_w from soundings and q_d as its corresponding saturation specific humidity at the surface. The free troposphere varies gradually, justifying the interpolation of 3-hourly sounding estimates of θ_d and q_d and of $\theta_{\rm en}$ and $q_{\rm en}$ to 1-min surface observations. Soundings show potential temperature at 800 m and wet-bulb potential temperature above 1.5 km are fairly insensitive to whether the temperature at the surface was influenced by a cold downdraft (de Szoeke et al. 2017). Moist static energy $h = c_p T + gz + Lq$, where c_p is specific heat, T is temperature, g is acceleration due to gravity, and L is latent heat, is calculated from θ and q for the BL and its end members.

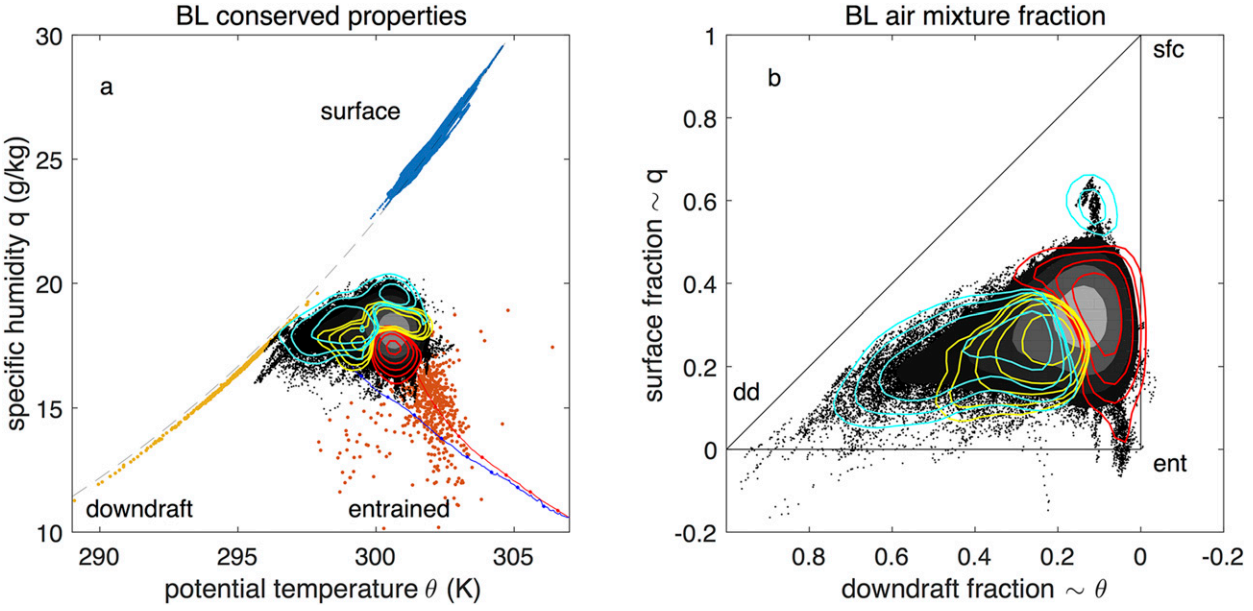

FIG. 2. (a) Potential temperature θ and specific humidity q in the BL (0–500 m; black dots and shaded probability density) and for end members from the ocean surface (blue), entrainment (z = 800 m; dark orange), and downdrafts (θ_w conserved from 3 km and its saturation specific humidity in BL; gold; after de Szoeke et al. 2017, their Fig. 11a). The dashed curve indicates water vapor saturation at 1004 hPa. (b) Mixing fractions of BL air from surface f_s and downdraft f_d end members deduced from θ and q. Filled contours show the average frequency density of BL observations. Unfilled contours show relative doublings of the frequency density in the convectively suppressed (red), disturbed (yellow), and active (cyan) intraseasonal convective phases.

b. *Transformation from conserved variables to mixing fractions and MSE fluxes*

The BL budget of a conserved variable h is composed of the fluxes from downdrafts, entrainment, and sea surface fluxes, plus a residual R:

$$\rho z_i \partial h_B/\partial t = W_d(h_d - h_B) + W_{\rm en}(h_{\rm en} - h_B) + W_s(h_s - h_B) + R, \quad (2)$$

where h_B is the MSE of the BL and h_d, $h_{\rm en}$, and h_s are the MSE of downdrafts, entrained air, and air at thermodynamic equilibrium with the ocean surface, respectively. The mass of the BL is ρz_i, the product of the air density and the BL depth. The MSE fluxes are factored as their respective mass fluxes W_d, $W_{\rm en}$, and W_s and the MSE difference of each end member relative to the BL air (depicted schematically in Fig. 1). The tendency is noisy but less than 0.1 W m^{-2} in the mean, so it is neglected. The effects of horizontal advection and radiation on the BL MSE are expected to be small (Thayer-Calder and Randall 2015; de Szoeke et al. 2017). The residual R includes these as well as the error. The downdraft, entrainment, and surface fluxes are larger than the residual.

The BL mixture of conserved properties θ_B and q_B is weighted by the mixing fractions $f_d = W_d/W_B$, $f_{\rm en} = W_{\rm en}/W_B$, and $f_s = W_s/W_B$; thus,

$$\begin{pmatrix} \theta_d & \theta_{\rm en} & \theta_s \\ q_d & q_{\rm en} & q_s \\ 1 & 1 & 1 \end{pmatrix} \begin{pmatrix} W_d/W_B \\ W_{\rm en}/W_B \\ W_s/W_B \end{pmatrix} = \begin{pmatrix} \theta_B \\ q_B \\ 1 \end{pmatrix}. \quad (3)$$

Each mixing fraction is the ratio of the mass flux to the total of all mass fluxes $W_B = W_d + W_{\rm en} + W_s$. Substituting $W_{\rm en}/W_B = 1 - W_d/W_B - W_s/W_B$ yields the two-dimensional system of differences in observed θ and q:

$$\begin{pmatrix} \theta_d - \theta_{\rm en} & \theta_s - \theta_{\rm en} \\ q_d - q_{\rm en} & q_s - q_{\rm en} \end{pmatrix} \begin{pmatrix} W_d/W_B \\ W_s/W_B \end{pmatrix} = \begin{pmatrix} \theta_B - \theta_{\rm en} \\ q_B - q_e \end{pmatrix}. \quad (4)$$

The two-dimensional matrix on the left-hand side of Eq. (4) rotates the mixing fractions (Fig. 2b) into the differences between the observed BL and entrainment potential temperature $\theta_B - \theta_{\rm en}$ and specific humidity $q_B - q_{\rm en}$ (Fig. 2a). The mixing fractions are solved for each observed realization of θ_d, $\theta_{\rm en}$, θ_s, θ_B, q_d, $q_{\rm en}$, q_s, and q_B.

The surface MSE flux is the sum of the sensible and latent surface heat fluxes, $F_s = H + E$, calculated from the bulk flux algorithm. From the surface MSE flux, we get the surface mass flux:

$$W_s = (H + E)/(h_s - h_B). \quad (5)$$

The downdraft and entrainment mass fluxes W_d and $W_{\rm en}$ are solved to be consistent with the mixing fractions and

TABLE 1. Mean BL MSE fluxes plus and minus the standard deviation of the mean (W m^{-2}) for all days and for convectively disturbed days (RMM phase 1), convectively active days (RMM phases 2 and 3), and convectively suppressed days (RMM phases 4–8). Negative fluxes represent MSE export from the BL. The number of 1-min realizations N and the factor $(1 - r)/(1 + r)$ that reduces the number of degrees of freedom (DOF) of the mean due to the autocorrelation r of the realizations are shown.

	All	Suppressed	Disturbed	Active	DOF factor
N	97 604	56 603	12 960	28 041	—
Downdraft	−62 ± 2	−49 ± 2	−60 ± 3	−87 ± 4	1.31×10^{-2}
Entrainment	−47 ± 1	−57 ± 1	−30 ± 2	−37 ± 2	2.34×10^{-2}
Surface	119 ± 4	116 ± 3	98 ± 5	136 ± 7	3.69×10^{-3}
Residual	−10 ± 5	−10 ± 4	−8 ± 6	−12 ± 8	—

the surface mass flux W_s. Finally, the mass fluxes are multiplied by the MSE differences to get the downdraft F_d and entrainment $F_{\rm en}$ moist static energy fluxes,

$$F_d = W_d(h_d - h_B), \tag{6}$$

$$F_{\rm en} = W_{\rm en}(h_{\rm en} - h_B). \tag{7}$$

The residual flux R is calculated assuming the tendency is zero.

The entrainment and downdraft MSE flux retrievals are not accurate when the relative surface mass flux, which appears in their denominator, becomes too small. Inverting Eq. (4) when $W_s/W_B < 0.03$ is ill posed because the relative error of the norm of the mixing fraction vector $(W_d, W_{\rm en}, W_s)/W_B$ is greater than one. Because these cases are so rare, removing fluxes when $W_s/W_B < 0.03$ changes the fluxes in Table 1 by less than 3 W m^{-2}.

The short 1-min averages need not have reached equilibrium, yet the vast majority of them are representative of a mixture of estimates of downdraft, entrained, and surface air. A small fraction, 0.5% of all 1-min observations, and 1.7% of those in the active phase, cannot be explained as a mixture of the three end members. In more than 90% of those cases, the BL observations are drier than either the downdraft or entrained air estimated from the soundings. This is consistent with soundings undersampling the driest air, perhaps from downdrafts with lower wet-bulb temperature.

3. Results

a. Equilibrium downdraft and entrainment fluxes

Figure 2a shows the scatterplot and joint density of all the 1-min boundary layer (θ_B and q_B) observations compared to the three end members: downdrafts (θ_d and q_d; yellow), entrainment ($\theta_{\rm en}$ and $q_{\rm en}$; red), and the surface (θ_s and q_s; blue). We linearly transform each realization from θ and q (Fig. 2a) to mixing fraction coordinates [f_d and f_s in Eq. (1); Fig. 2b]. Downdrafts and entrained air have similar specific humidity, slightly drier than the BL, so the partition between downdrafts and entrainment mass fluxes is largely determined by potential temperature. The potential temperature of the sea surface and entrained air are similar and slightly warmer than the BL.

Both entrainment and downdrafts export significant MSE from the BL in order to explain the observed budget (Figs. 3a,c). Downdraft MSE flux is more variable and stronger during convectively active periods. Infrequent strong downdraft MSE flux gives its probability density a long negative tail (Fig. 3c) that makes it more negative in the mean than the entrainment flux (Table 1). The mean surface MSE flux of 120 W m^{-2} into the BL is balanced mostly by −60 W m^{-2} MSE flux (export) by saturated downdrafts and −50 W m^{-2} by entrainment of dry air with the properties of 800 m.

The small residual MSE export of less than −10 W m^{-2} suggests introduction of colder saturated downdrafts or colder and drier entrained air not sampled by the sparse soundings. Weak cold and dry BL advection from cooler to warmer regions may also contribute to the residual (Halley 1686; Lindzen and Nigam 1987; Back and Bretherton 2009). Horizontal advection in the BL, estimated from the DYNAMO northern sounding array (Johnson and Ciesielski 2013), is negative and smaller than our residual, about −2 W m^{-2} on average (Sobel et al. 2014, their Fig. 6c). It reaches a maximum of −9 W m^{-2} under the active convection in late November. Vertical advection is negligible in the BL. Our residual is larger than can be explained by the advection but small relative to the other MSE fluxes in our calculation. The method for estimating the relative mass fluxes assumes the BL properties are an equilibrium mixture of the three end members. The smallness of the standard error of the mean and of the residual MSE flux indicates the accuracy of the MSE fluxes from this equilibrium budget.

b. Intraseasonal variability

The MSE fluxes into the BL are averaged for each of the convectively suppressed, disturbed, and active phases of the MJO (de Szoeke et al. 2017), defined by the real-time multivariate MJO index (RMM; Wheeler and Hendon 2004) found by projection of global tropical

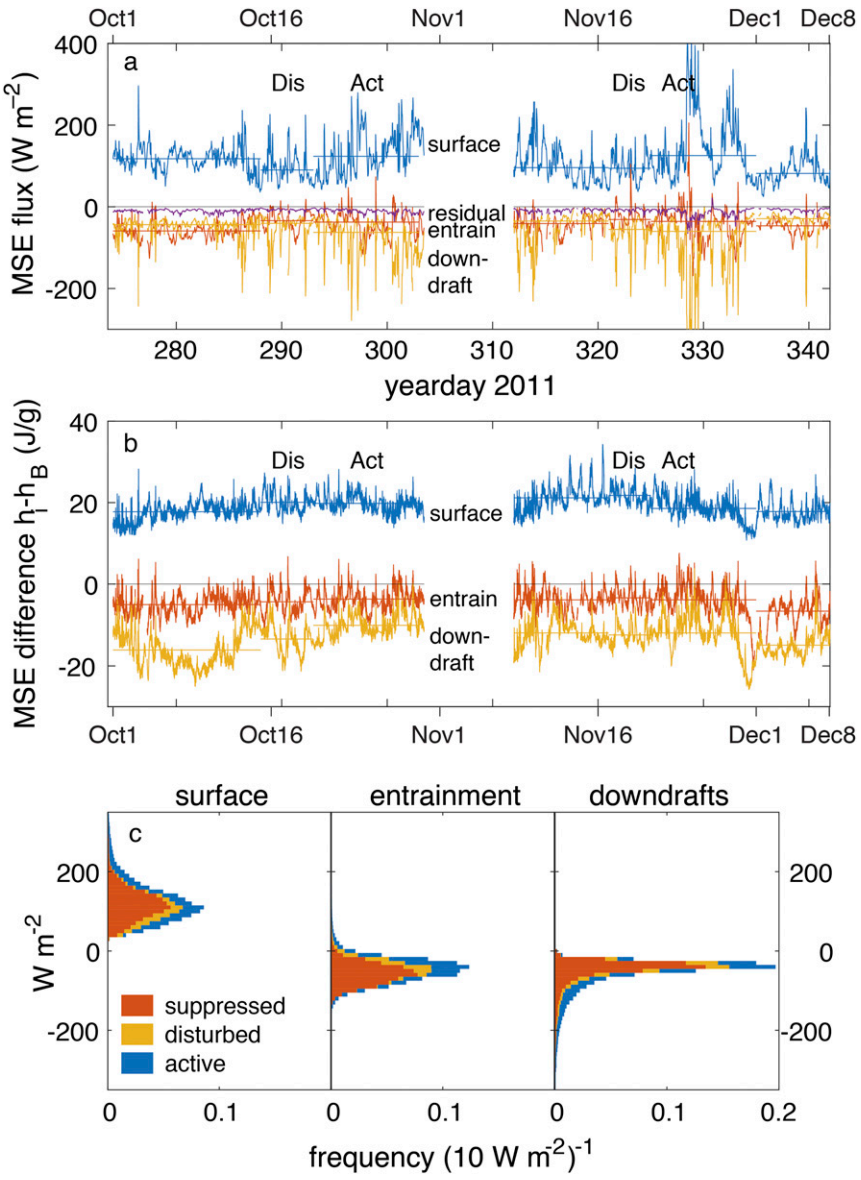

FIG. 3. (a) The 1-h median MSE flux due to surface sensible and latent heat fluxes (gold), entrainment (dark orange), saturated downdrafts from the midtroposphere (blue), and the residual (purple) over the *Revelle* in the central Indian Ocean for legs 2 and 3 of DYNAMO. (b) Difference between the MSE h_i of the end member i and the MSE h_B of the BL. Horizontal lines indicate averages over continuous intervals of days of suppressed, disturbed (Dis), and active (Act) convection according to the phase of the RMM intraseasonal index. (c) Probability density of the (left) surface, (center) entrainment, and (right) downdraft MSE flux, stacked horizontally according to their intraseasonal phase: suppressed (dark orange), disturbed (gold), and active (blue).

outgoing longwave radiation and zonal wind onto their intraseasonal modes of variability. RMM phase 1, prior to the intraseasonal phase of active deep convection, is described as convectively *disturbed*. RMM phases 2 and 3 have the deepest convection and are described as convectively *active*. The remaining RMM phases (4–8) have the least convection and are described as convectively *suppressed*.

Mean entrainment and saturated downdraft MSE fluxes are comparable during the suppressed phase of the MJO (Table 1). Downdraft MSE export increases to twice the entrainment in the disturbed phase and 2.3

times the entrainment in the convectively active phase. The entrainment MSE export decreases in the convectively disturbed and active phases because entrained air from above the BL is moister in these phases. Intraseasonal convective events observed in the central Indian Ocean at 0°, 80°E in summer 2011 during DYNAMO were anomalously strong (de Szoeke et al. 2015).

Downdrafts have a greater influence on the BL in the convectively active phase. Unfilled contours in Fig. 2b show the increase of the probability density of mixing fraction in the convectively active (cyan; RMM phases 2–3), disturbed (yellow; RMM phase 1), and suppressed (red; RMM phases 4–8) phases of the MJO relative to the mean probability density. Probability density of θ and q (Fig. 2a) is enhanced in two separate modes in the convective phase, one moister and one cooler, because of large correlated variations of the specific humidity of the entrained air and the surface. These two modes merge in the mixing fraction probability density (Fig. 2b).

4. Summary

Entrained air and saturated downdrafts have similar potential temperature above the boundary layer, yet downdrafts become cooler because of evaporation of clouds and rain. This analysis is consistent with downdraft covariance fluxes computed by conditioning on cloudy and rainy areas in models (Thayer-Calder and Randall 2015).

Downdraft MSE flux from the boundary layer to the free troposphere is 40% higher than average in the convective phase of the MJO. This study shows that the formulation of the BL equilibrium must include the effect of entrainment of warm and dry lower-tropospheric air into the BL but that downdraft MSE export dominates entrainment drying by a factor of ~2 in intraseasonal convective events. The ability of local surface flux, downdraft flux, and entrainment flux to explain BL MSE supports the theory of BL quasi equilibrium for the interaction of convection with the BL (Raymond 1995).

Models and observations suggest the increase of free-tropospheric moisture by detrainment from midlevel convection before or during the convective phase of the MJO (Bladé and Hartmann 1993; Kemball-Cook and Weare 2001; Benedict and Randall 2007; Powell and Houze 2013). Fluxes of moisture, parameterized in general circulation models, can be assessed directly by eddy covariance in cloud-permitting models, and these model results can be constrained by verification against observations of the BL budgets of conserved variables. The conserved variables also constrain direct estimates of MSE fluxes at the BL top by remote sensing.

Noting relatively uniform temperature of the tropical atmosphere (Sobel et al. 2001), moisture-mode theories (e.g., Sugiyama 2009; Raymond and Fuchs 2009; Chikira 2014) emphasize feedbacks to tropospheric moisture for creating unstable intraseasonal convective modes in the column MSE budget. The tropical intraseasonal skeleton model of Majda and Stechmann (2009) suggests that BL moisture east of the area of active MJO convection stimulates synoptic wave activity that supports the spatial structure of the MJO. The (Wang et al. 2016) trio-interaction theory for the MJO explores interactions among convection, moisture, and BL wave dynamics. Moisture anomalies east of the peak of convection (Sobel and Maloney 2013; Adames and Kim 2016; Fuchs and Raymond 2017) contribute to the growth and eastward propagation of long-wavelength planetary convective anomalies. Intraseasonal variation of the surface fluxes, mostly due to the wind speed, is only ~10% of the mean evaporation (de Szoeke et al. 2015) and has a relatively small effect on the MSE budget of the BL. The small negative (drying) horizontal advection inferred from the DYNAMO soundings (Sobel et al. 2014) and the small negative residual in our local MSE budget imply that advective moistening is not a major term in the BL MSE budget in any phase.

Acknowledgments. The author is grateful for helpful discussions in the early stages of this work with Drs. P. Zuidema and E. D. Skyllingstad and for the insightful comments from the two anonymous reviewers. The author acknowledges support from NOAA Climate Program Office CVP Grants NA15OAR4310242 and NA13OAR4310160 and the ONR PISTON DRI Grant N00014-16-1-3094. DYNAMO surface meteorology and flux data are available from NOAA/ESRL/PSD or University of Connecticut (ftp://dynamo.dms.uconn.edu/) data repositories. Sounding data are available at the University Corporation for Atmospheric Research Earth Observing Laboratory data website (http://data.eol.ucar.edu/dataset/347.158).

REFERENCES

Adames, Á. F., and D. Kim, 2016: The MJO as a dispersive, convectively coupled moisture wave: Theory and observations. *J. Atmos. Sci.*, **73**, 913–941, https://doi.org/10.1175/JAS-D-15-0170.1.

Arakawa, A., and W. H. Schubert, 1974: Interaction of a cumulus cloud ensemble with the large-scale environment, part I. *J. Atmos. Sci.*, **31**, 674–701, https://doi.org/10.1175/1520-0469(1974)031<0674:IOACCE>2.0.CO;2.

Back, L. E., and C. S. Bretherton, 2009: On the relationship between SST gradients, boundary layer winds, and convergence over the tropical oceans. *J. Climate*, **22**, 4182–4196, https://doi.org/10.1175/2009JCLI2392.1.

Benedict, J. J., and D. A. Randall, 2007: Observed characteristics of the MJO relative to maximum rainfall. *J. Atmos. Sci.*, **64**, 2332–2354, https://doi.org/10.1175/JAS3968.1.

Betts, A. K., 1976: Modeling subcloud layer structure and interaction with a shallow cumulus layer. *J. Atmos. Sci.*, **33**, 2363–2382, https://doi.org/10.1175/1520-0469(1976)033<2363:MSLSAI>2.0.CO;2.

Bladé, I., and D. L. Hartmann, 1993: Tropical intraseasonal oscillations in a simple nonlinear model. *J. Atmos. Sci.*, **50**, 2922–2939, https://doi.org/10.1175/1520-0469(1993)050<2922:TIOIAS>2.0.CO;2.

Chikira, M., 2014: Eastward-propagating intraseasonal oscillation represented by Chikira–Sugiyama cumulus parameterization. Part II: Understanding moisture variation under weak temperature gradient balance. *J. Atmos. Sci.*, **71**, 615–639, https://doi.org/10.1175/JAS-D-13-038.1.

Ciesielski, P. E., 2014: R/V Roger Revelle radiosonde L3.1 data (ESC format). Earth Observing Laboratory, accessed 15 March 2014, http://data.eol.ucar.edu/dataset/347.158.

DeMott, C. A., N. P. Klingaman, and S. J. Woolnough, 2015: Atmosphere-ocean coupled processes in the Madden-Julian oscillation. *Rev. Geophys.*, **53**, 1099–1154, https://doi.org/10.1002/2014RG000478.

de Szoeke, S. P., J. B. Edson, J. R. Marion, C. W. Fairall, and L. Bariteau, 2015: The MJO and air–sea interaction in TOGA COARE and DYNAMO. *J. Climate*, **28**, 597–622, https://doi.org/10.1175/JCLI-D-14-00477.1.

——, E. D. Skyllingstad, P. Zuidema, and A. S. Chandra, 2017: Cold pools and their influence on the tropical marine boundary layer. *J. Atmos. Sci.*, **74**, 1149–1168, https://doi.org/10.1175/JAS-D-16-0264.1.

Edson, J. B., and Coauthors, 2013: On the exchange of momentum over the open ocean. *J. Phys. Oceanogr.*, **43**, 1589–1610, https://doi.org/10.1175/JPO-D-12-0173.1.

Fletcher, J. K., and C. S. Bretherton, 2010: Evaluating boundary layer–based mass flux closures using cloud-resolving model simulations of deep convection. *J. Atmos. Sci.*, **67**, 2212–2225, https://doi.org/10.1175/2010JAS3328.1.

Fuchs, Ž., and D. J. Raymond, 2017: A simple model of intraseasonal oscillations. *J. Adv. Model. Earth Syst.*, **9**, 1195–1211, https://doi.org/10.1002/2017MS000963.

Halley, E., 1686: An historical account of the trade winds, and monsoons, observable in the seas between and near the tropicks, with an attempt to assign the physical cause of the said winds. *Philos. Trans.*, **16**, 153–168, https://doi.org/10.1098/rstl.1686.0026.

Johnson, R. H., and P. E. Ciesielski, 2013: Structure and properties of Madden–Julian oscillations deduced from DYNAMO sounding arrays. *J. Atmos. Sci.*, **70**, 3157–3179, https://doi.org/10.1175/JAS-D-13-065.1.

Kemball-Cook, S. R., and B. C. Weare, 2001: The onset of convection in the Madden–Julian oscillation. *J. Climate*, **14**, 780–793, https://doi.org/10.1175/1520-0442(2001)014<0780:TOOCIT>2.0.CO;2.

Lindzen, R. S., and S. Nigam, 1987: On the role of sea surface temperature gradients in forcing low-level winds and convergence in the tropics. *J. Atmos. Sci.*, **44**, 2418–2436, https://doi.org/10.1175/1520-0469(1987)044<2418:OTROSS>2.0.CO;2.

Madden, R. A., and P. R. Julian, 1971: Detection of a 40–50 day oscillation in the zonal wind in the tropical Pacific. *J. Atmos. Sci.*, **28**, 702–708, https://doi.org/10.1175/1520-0469(1971)028<0702:DOADOI>2.0.CO;2.

Majda, A. J., and S. N. Stechmann, 2009: The skeleton of tropical intraseasonal oscillations. *Proc. Natl. Acad. Sci. USA*, **106**, 8417–8422, https://doi.org/10.1073/pnas.0903367106.

Mapes, B. E., 2000: Convective inhibition, subgrid-scale triggering energy, and stratiform instability in a toy tropical wave model. *J. Atmos. Sci.*, **57**, 1515–1535, https://doi.org/10.1175/1520-0469(2000)057<1515:CISSTE>2.0.CO;2.

Neelin, J. D., and N. Zeng, 2000: A quasi-equilibrium tropical circulation model—Formulation. *J. Atmos. Sci.*, **57**, 1741–1766, https://doi.org/10.1175/1520-0469(2000)057<1741:AQETCM>2.0.CO;2.

Powell, S. W., and R. A. Houze Jr., 2013: The cloud population and onset of the Madden-Julian oscillation over the Indian Ocean during DYNAMO-AMIE. *J. Geophys. Res. Atmos.*, **118**, 11 979–11 995, https://doi.org/10.1002/2013JD020421.

Raymond, D. J., 1995: Regulation of moist convection over the west Pacific warm pool. *J. Atmos. Sci.*, **52**, 3945–3959, https://doi.org/10.1175/1520-0469(1995)052<3945:ROMCOT>2.0.CO;2.

——, and Ž. Fuchs, 2009: Moisture modes and the Madden–Julian oscillation. *J. Climate*, **22**, 3031–3046, https://doi.org/10.1175/2008JCLI2739.1.

Sherwood, S. C., S. Bony, and J.-L. Dufresne, 2014: Spread in model climate sensitivity traced to atmospheric convective mixing. *Nature*, **505**, 37–42, https://doi.org/10.1038/nature12829.

Sobel, A., and E. Maloney, 2013: Moisture modes and the eastward propagation of the MJO. *J. Atmos. Sci.*, **70**, 187–192, https://doi.org/10.1175/JAS-D-12-0189.1.

——, J. Nilsson, and L. M. Polvani, 2001: The weak temperature gradient approximation and balanced tropical moisture waves. *J. Atmos. Sci.*, **58**, 3650–3665, https://doi.org/10.1175/1520-0469(2001)058<3650:TWTGAA>2.0.CO;2.

——, S. Wang, and D. Kim, 2014: Moist static energy budget of the MJO during DYNAMO. *J. Atmos. Sci.*, **71**, 4276–4291, https://doi.org/10.1175/JAS-D-14-0052.1.

Sugiyama, M., 2009: The moisture mode in the quasi-equilibrium tropical circulation model. Part I: Analysis based on the weak temperature gradient approximation. *J. Atmos. Sci.*, **66**, 1507–1523, https://doi.org/10.1175/2008JAS2690.1.

Thayer-Calder, K., and D. Randall, 2015: A numerical investigation of boundary layer quasi-equilibrium. *Geophys. Res. Lett.*, **42**, 550–556, https://doi.org/10.1002/2014GL062649.

Wang, B., F. Liu, and G. Chen, 2016: A trio-interaction theory for Madden–Julian oscillation. *Geosci. Lett.*, **3**, 34, https://doi.org/10.1186/s40562-016-0066-z.

Wheeler, M. C., and H. H. Hendon, 2004: An all-season real-time multivariate MJO index: Development of an index for monitoring and prediction. *Mon. Wea. Rev.*, **132**, 1917–1932, https://doi.org/10.1175/1520-0493(2004)132<1917:AARMMI>2.0.CO;2.

Yoneyama, K., C. Zhang, and C. N. Long, 2013: Tracking pulses of the Madden–Julian oscillation. *Bull. Amer. Meteor. Soc.*, **94**, 1871–1891, https://doi.org/10.1175/BAMS-D-12-00157.1.

Zhang, G. J., and N. A. McFarlane, 1995: Sensitivity of climate simulations to the parameterization of cumulus convection in the Canadian Climate Centre general circulation model. *Atmos.–Ocean*, **33**, 407–446, https://doi.org/10.1080/07055900.1995.9649539.

Zuidema, P., and Coauthors, 2012: On trade wind cumulus cold pools. *J. Atmos. Sci.*, **69**, 258–280, https://doi.org/10.1175/JAS-D-11-0143.1.